Simulating typhoon-induced storm hydrographs in subtropical mountainous watershed: an integrated 3-layer TOPMODEL

J.-C. Huang, T.-Y. Lee, S.-J. Kao

Hydrology and Earth System Sciences Discussions

Simulating typhoon-induced storm hydrographs in subtropical mountainous watershed: an integrated 3-layer TOPMODEL

J.-C. Huang[1], T.-Y. Lee[1,2], and S.-J. Kao[1]

[1]Research Center for Environmental Changes, Academia Sinica, Taipei, Taiwan
[2]Dept. of Bioenvironmental Systems Engineering, National Taiwan University, Taipei, Taiwan

HESSD

5, 1101–1135, 2008

An integrated 3-layer TOPMODEL

Jr-Chuan Huang et al.

Title Page

Abstract	Introduction
Conclusions	References
Tables	Figures

◄◄ ►►

◄ ►

Back Close

Full Screen / Esc

Printer-friendly Version

Interactive Discussion

Abstract

A three-layer TOPMODEL is here constructed by integrating three components, diffusion wave approach into surface flow, soil moisture deficit into interflow and exponential recession curve function into base flow. Sensitivity analysis reveals that D (soil depth), K (hydraulic conductivity), and m_i (soil moisture decay) predominate simulated hydrograph shape and total discharge, yet, there are distinct effects on the three flows. A subtropical mountainous watershed, Heng-Chi and eighteen typhoon-induced storms with various rainfall type and wide-ranged total rainfall (81 to 1026 mm) were applied. The global best-fitted combination gives an average efficient coefficient of 75.1% and 76.0% for calibration (14 cases) and validation (4 cases), respectively. Most discharges of validation events fall within the 90% confidence interval derived from calibration events. Those results demonstrate the capability of the 3-layer TOPMODEL in subtropical watershed. Meanwhile, the upper confidence limit is suggested preferably when considering the flood assessment.

1 Introduction

Located along the typhoon alley in the western Pacific, Island Taiwan averages 4 annual typhoon invasions from June to October (Taiwan Central Weather Bureau, www.cwb.gov.tw), which bring abrupt heavy rainfalls in summer. Coupled with steep landscape morphology and fracture rocks, typhoon-induced debris flows and landslides often occur at upstream and flood at downstream area. For instances, Herb Typhoon in 1996, Zeb Typhoon in 1998 and Xangsane Typhoon in 2000 brought over 800 mm rainfall within 2 d. Nari Typhoon in 2001 broke the record by bringing 1026 mm within 2 d with rainfall intensity over 50.0 mm/h in certain hours. This event hammered Taipei City (Sui et al., 2002). More than 400 landslides were triggered in Taipei Basin and the low land city areas were severely flooded. It also took 94 human lives. Total economic loss was about 9 billion NT dollars (Sui et al., 2002). Those typhoons and related hazards

not only seriously threaten human lives they also result in an average annual loss of more than 500 million US dollars in terms of agricultural, economical, and infrastructure damages (Li et al., 2005). Simulating hydrological responses (e.g. stream discharge) is thus one of the major concerns for hazard mitigation and water resource manage-
5 ment in Taiwan and in other countries for analogous climate research. Recent research suggests that as a result of climate fluctuations there could have been an increasing western Pacific cyclone frequency (Wu et al., 2005). Taiwan and other regions in East Asia are now experiencing a greater influence of typhoons. A suitable hydrological model is urgently needed.

10   However, to simulate dramatic responses of storm hydrograph in mountainous watersheds in Taiwan is challenging due to short river channel and complex terrain. A popular watershed modeling tool, "TOPMODEL" (Beven, 2001), has been demonstrated applicable to a wide variety of climates and landscapes (e.g. Lamb et al., 1998; Scanlon et al., 2000) because of its simplicity and clever use of geomorphology. In spite
15 of complicated calculations and assumptions, TOPMODEL simulates subsurface flow (including interflow and base flow) by applying exponential recession curve function which is simple and effective. On the other hand, TOPMODEL introduces the topographic index to describe the water table deficit at any point inside the watershed. Topography has been recognized as an important factor in determining runoff gener-
20 ation in mountainous watersheds, particularly for those with relatively shallow soils in wet conditions (Beven, 2001). Linking the topographic index and recession curve function by catchment storage concept, TOPMODEL can simultaneously simulate stream discharge and spatial pattern of water table deficit (or soil wetness). The latter part can also be incorporated into landslide modeling (Huang et al., 2006).

25   Many recent studies indicated that separating subsurface flow into interflow and base flow can better simulate stream discharge in dry condition with short and intensive rainfall (e.g. humid tropical climate by Campling et al., 2002; Mediterranean climate by Candela et al., 2005). Various process related to modifications have been proposed previously (Scanlon et al., 2000; Hornberger et al., 2001; Walter et al., 2002). On

the other hand, in order to improve the estimation of surface flow convolution, routing procedure have also been introduced into TOPMODEL to specify the drainage path and travel time of each cell (Candela et al., 2005). In this regard, many applications onto different climate and landscape conditions have well been discussed (reviewed by Beven, 1997). As aforementioned, typhoon invades episodically in summer when soil is dry and water discharge is low in Taiwan. However, none of them was documented in the TOPMODEL performance for frequent typhoon-induced extreme rainfall storms in subtropical region and none of the applications was integrated with advanced modifications mentioned above as a whole.

Integrating with previous modifications, this study aims to construct a 3-layer TOPMODEL for subtropical small mountainous watersheds, particularly for simulating flood discharges caused by typhoons. Firstly, sensitivity analysis was carried out to unravel major controlling parameters and the interactions of the three components (surface flow, interflow, and base flow). Secondly, Heng-Chi, one of small watersheds at northern Taiwan, was applied. Fourteen extreme events during 1990–2000 were selected for calibration and the other four (during 2001–2004) for subsequent validation. 20 000 parameter sets generated by random number were conducted to single out the global best-fitted combination. Meanwhile, we compared all observed discharges to simulated discharges among calibration events to extract the confidence intervals. The entire procedure would advance the understanding of model structure and benefit further decision-making in hazard mitigation program and TOPMODEL applications in subtropical region.

2   Materials

2.1   Study area

The climate in northern Taiwan is characterized by wet winters and dry summers with frequent typhoons in July, August and September. Average annual precipitation varies

Title Page

Abstract | Introduction

Conclusions | References

Tables | Figures

◄ | ►

◄ | ►

Back | Close

Full Screen / Esc

Printer-friendly Version

Interactive Discussion

from 2500 mm to 3100 mm and the mean monthly temperature ranges from 13°C in January to 28°C in July (Taiwan Central Weather Bureau).

Heng-Chi with a drainage area of 52.10 km^2 (Fig. 1) has its main stream originated from Xiong-Kong Mt. (960 m a.s.l.). It is a tributary of Danshusi River, which flows through Taipei City where upholds over 2.65 million residents. High population density in Taipei City underscores the importance of hydrological modeling for upstream tributaries that may contribute to downstream flood warning and hazard mitigation. Elevations of the catchment range from 180 to 960 m with an average slope of 41.1%. The topographic map and gauging stations are also shown in Fig. 1. One hydrological station and only one rainfall station inside the watershed are maintained by the Water Resource Agency (WRA, www.wra.gov.tw). The geology in Heng-Chi watershed is mainly composed of sandstone and shale (Taiwan Central Geological Survey, www.moeacgs.gov.tw). Strong weathering and prevailing erosion in this region created steep and deeply dissected landscape. Slopelands and low hills which veneered by gravelly and sandy loam soils occupy 90% of the area. Rice fields and some farm houses occupy gentle slopes at lower elevation while shrubbery, bamboo and primeval forest take up slopes at higher elevation.

2.2 Extreme rain storms and flood events

The basic characteristics of the 18 storm events are selected for this study (Table 1). Event total rainfall ranges from 81 to 1026 mm with an average rainfall intensity of 5.7~20.8 mm/h and the maximum rainfall intensity of 20.0~61.0 mm/h. In most cases, cumulative rainfalls are over 300 mm within 34 h. The total discharge ranges from 869 to 15 241 cms positively correlating with event total rainfall. The peak flow ranges from 68.6 to 870.0 cms without obvious correlation to total rainfall and rainfall intensity (Table 1). Water discharge responds rapidly to rainfall of short lag times (generally less than 2 h). Averagely speaking, the discharge surges approximately 200x, from <1.5 cms to >271 cms within one hour. To investigate the model capability for unknown events, we select 14 events during 1990–2000 for calibration and 4 events

during 2001–2004 for validation. Note that the largest event, event 16, and shortest one, event 15, are excluded for calibrating purpose.

3 Methods

3.1 Three-layer structure and model formulation

The three-layer TOPMODEL contains eight processes: precipitation, evapotranspiration, interception, infiltration, percolation, surface flow, interflow and base flow (in Fig. 2). Storage organization consists of three layers: 1) the upper layer, that is, the Root Zone, which has a fixed maximum water storage capacity, S_{1max} (L), and state variable of upper layer storage, S_1 (L); 2) the middle layer, which is the conventional Unsaturated Zone between ground surface and the ground water table, with soil moisture deficit, S_D, (L) as state variable (detailed below); 3) the bottom layer, the Saturated Zone, below the ground water table with S_3 (L) as its storage. The three state variables are used to regulate the surface flow (Q_s), inter-flow (Q_i) and base flow (Q_b). Relations among vertical flow, horizontal flow and state variables are illustrated below.

When the rain falls, it is initially stored in the upper layer, where evapotranspiration occurs. Accordingly, storage, S_1, in the upper layer is controlled by rainfall and actual evapotranspiration (E_a), which is determined by the ratio of S_1 to S_{1max} and potential evapotranspiration (E_p) at the previous time step. The formula of E_a (L/T) is given below:

$$E_a = E_p \frac{S_1}{S_{1\,max}}, \tag{1}$$

The potential evapotranspiration can be estimated by many methods (e.g. Penman, 1948; Monteith, 1965). Here we applied the most economical empirical approximation (not shown; detailed in Casadai et al., 2003) proposed by Hamon (1961). The potential evapotranspiration estimation is off-line in storm simulation because the storm period

An integrated 3-layer TOPMODEL

Jr-Chuan Huang et al.

Title Page

Abstract	Introduction
Conclusions	References
Tables	Figures

|◄ | ►|

◄ | ►

Back | Close

Full Screen / Esc

Printer-friendly Version

Interactive Discussion

is relatively short (less than 3 d) and the vapor pressure is almost saturated as raining. Once S_1 exceeds $S_{1\,max}$ due to rainfall, the excess, q_r (L), infiltrates vertically down into the middle layer to increase soil moisture before the middle layer is fully saturated; after saturation state is reached the surplus q_r flow horizontally into Q_s, in the mean time, a

5   vertical flux, P, percolates into the bottom layer from middle layer to elevate the bottom layer storage, S_3. In each time step, S_D and S_3 are used to calculate, respectively the Q_i and Q_b. The calculations of the surface flow, inter-flow and base flow are based on routing procedure described below.

For surface flow, we applied the flow path unit response function (Eq. 2) recently pro-

10   posed by Liu et al. (2003). Mannings' equation and energy dissipation theory (Molnar and Ramirez, 1998) were used to approach diffusion wave solution approximately.

The approximate solution is

$$U(t) = \frac{1}{\sigma\sqrt{2\pi \cdot t^3/t_0^3}} \exp\left[-\frac{(t - t_0)^2}{2\sigma^2 \cdot t/t_0}\right], \qquad (2)$$

where U(t) ($1/T$) is the flow path unit response function; t_0 (T) is the average travel

15   time of the cell to outlet along flow path and σ (T) is the standard deviation of the flow time. The spatially distributed parameters t_0 and σ are retrieved from DEMs (40-m resolution). Accordingly, each flow path has different parameters depending on the length of the flow path and the physical characteristics of the flow path element. Note that Mannings' surface roughness, n, is embedded implicitly in the above equation.

20   The total surface flow hydrograph at the watershed outlet is obtained by a convolution integral of the flow response from all grid cells.

For inter flow, Q_i (L^3/T), we followed the formula in original TOPMODEL:

$$\begin{array}{l} Q_i = Q_0 \exp(-m_i\overline{S_D}) \\ Q_0 = A \exp(-\lambda) \end{array}, \qquad (3)$$

where Q_0 is defined as a outflow parameter related to soil hydraulic properties and

25   topography; m_i is the soil characteristic parameter; A is the watershed area and λ is

An integrated 3-layer TOPMODEL

Jr-Chuan Huang et al.

Printer-friendly Version

Interactive Discussion

the averaged topographic index (see below) of the entire watershed. $\overline{S_D}$ is the area average of soil moisture deficit for the entire watershed. Q_0 (L^3/T) is the discharge when soil moisture deficit equals zero. The soil moisture deficit is the reduced moisture deficit per unit volume of soil from saturation (Walter et al., 2002):

$$S_D = 1 - \frac{\theta - \theta_d}{\theta_s - \theta_d}, \tag{4}$$

where θ is the average soil moisture content, θ_s is the saturated soil moisture content, θ_d is the air dry soil moisture content. Following the steady state assumption in TOPMODEL, the soil moisture deficit for each grid is:

$$S_{D,i} = \overline{S_D} + \frac{1}{m_i} \left[\lambda - \ln(\frac{a_i}{T_0 \tan \beta_i}) \right], \tag{5}$$

where $S_{D,i}$ and a_i (L) are the soil moisture deficit and specific contributing area for ith cell, respectively. The specific contributing area is derived from the infinite flow direction (Tarboton, 1997). Meanwhile the local slope gradient, β_i is calculated by Zevenbergen and Throne's method (1987). T_0 is the soil transmissivity defined as the product of hydraulic conductivity, K (L/T) and soil depth, D (L). λ equals $\frac{1}{A} \sum_i A_i \cdot \ln \frac{a_i}{T_0 \tan \beta_i}$ describing the averaged topographic index of the entire watershed.

For base flow calculation, Q_b, the exponential recession curve function is applied (Lamb and Beven, 1997):

$$Q_b = Q_0 \exp(-m_b \cdot S_3), \tag{6}$$

where m_b is the recession coefficient, and S_3 is the bottom layer storage. The initial bottom layer storage is represented as following:

$$S_{3,t=0} = -\frac{1}{m_b} \ln(\frac{Q_{t=0}}{Q_0}), \tag{7}$$

An integrated 3-layer TOPMODEL

Jr-Chuan Huang et al.

Full Screen / Esc

Printer-friendly Version

Interactive Discussion

where $Q_{t=0}$ is the initial discharge given in accordance with observed discharge. Therefore, S_3 can be determined at the first time step. Above three flows can be simulated step by step while hourly rainfall is applied.

Collectively, eight global variables in functions mentioned above are essential to route the model: surface roughness (n), maximum storage ($S_{1\,max}$) in the upper layer, initial value of (S_{10}), soil characteristic parameter (m_i), soil depth (D), hydraulic conductivity (K), base flow recession coefficient (m_b), and percolation rate (P). The main model outputs for each time step include the spatial pattern of soil moisture for the entire watershed and stream discharge at the outlet that composes of simulated surface flow, interflow and base flow.

TOPMODEL is a spatially distributed model. Many studies using distributed approach apply landuse map, soil map, and vegetation cover to represent the distributed parameter values. Those distributed maps introduce their information mainly according to classification but the information about parameters for each classification may be highly uncertain and may not be independent (Wang et al., 2006). On the other hand, those parameter values retrieved from parameter calibration are hard to validate in watershed scale due to scale dependence in parameter and inter-correlation among parameters (Beven, 2001; Huang et al., 2006). Since this study aims to resolve the most sensitive parameters governing the shape and total discharge of flood hydrographs, all parameters are assumed homogeneous. This uniform assumption reduces the complexity of heterogeneity and allows us to discriminate differences among all simulations subject to parameter changes.

3.2 Parameter calibration and performance measure

Parameter calibration is essential because of both the limitations of model structure and data availability of parameters, namely, initial conditions and boundary conditions (Beven, 2001). To quantify the performance of hydrological simulation prior to calibration, various measures were proposed depending on purpose such as hydrograph shape, peak flow, peak time, discharge volume or even low flow (e.g. Krause et al.,

2005; Madsen, 2000). Different measures, apparently, may extract different satisfying combinations for their own aspect.

Here, we combine the overall root mean square error (ORMSE) and average root mean square error of peak flow (ARMSE) with equal weights (Madsen, 2000) to serve as our performance measure (CRMSE). The following formulas define ORMSE, ARMSE, and CRMSE:

$$ORMSE = \left[\frac{\sum_{i=1}^{N} w_i^2 \left[Q_{s,i} - Q_{o,i} \right]^2}{\sum_{i=1}^{N} w_i^2} \right]^{1/2}, \tag{8}$$

$$ARMSE = \frac{1}{M_p} \sum_{j=1}^{M_p} \left[\frac{\sum_{i=1}^{n_j} w_i^2 \left[Q_{s,i} - Q_{o,i} \right]^2}{\sum_{i=1}^{n_j} w_i^2} \right]^{1/2}, \tag{9}$$

$$CRMSE = \frac{1}{2}ORMSE + \frac{1}{2}ARMSE, \tag{10}$$

In Eqs. (8)–(9), $Q_{o,i}$ is the observed discharge at time i, $Q_{s,i}$ the simulated discharge, N the total number of time steps in the individual events, M_p the number of peak flow events, n_j is the number of time steps in peak flow periods and w_i is the weighting function. Peak flow periods are defined as periods when the observed discharge is over 100 cms. According to above formulas, CRMSE concerns both the hydrograph shapes and peak flows, which are two major elements for flood warning.

To present differences between simulation and observation, we further provide 5 indicators, namely: EC, EC_{log}, EQV, EQP, and EQT. All five indicators are often used in evaluating hydrograph simulation. The efficiency coefficient (EC) proposed by Nash

and Sutcliffe (1970) can quantify the overall deviation between simulated and observed hydrographs. The highest value of *EC* is 1.0. To better quantify the similarity in low flow condition, EC_{log}, the logarithmic Nash-Sutcliffe efficient (e.g., Güntner et al., 1999; De Smedt et al., 2000), is suggested due to its ability to reproduce time evolution of low discharge. The other three indicators: the error of total discharge volume (*EQV*) is defined as the ratio of simulated total flow over observed total flow; the error of peak flow (*EQP*) is defined as the ratio of simulated peak flow over observed peak flow and the error of time to peak (*EQT*) is defined as the deviation between times of simulated peak and observed peak. Through the five indicators we broadly examine the performance of our simulations. In the following section, we illustrate the calibration procedures for extraction of the global best-fitted combination.

In this study, 20 000 parameter sets are generated by using uniform distribution (Table 2). The uniform distribution is generally accepted for generating parameters values when information for the parameter population in model simulation is insufficient. Basing on the 20 000 parameter combinations we run the model for all 14 events; thus 20 000 predictions and correspondent CRMSE values for each event are acquired. Among the 20 000 predictions we obtain the best-fitted combination (with lowest CRMSE value) for each event individually. However, the best-fitted combination may not be the best for the other events; we therefore summarize 14 event-correspondent CRMSE values to evaluate the overall performance of the respective parameter set. This overall performance acts as a criterion to single out the global best-fitted combination.

4 Results and discussion

4.1 Sensitive parameters in simulating hydrograph and discharge

A sensitivity analysis is performed by changing ±50.0% in single parameter while leaving others unchanged in the global best-fitted combination to examine the hydrograph

responses, which include the three components, surface flow, interflow, base flow, and the total discharge (Fig. 3). Event 5, which has the longest flood duration, is used as an example to present how we identify the sensitivity of parameters. Figure 3a and b clearly indicate that $S_{1\,max}$ and S_{10} affect the initial discharge only. The two parameters
5   which represent the maximum available upper layer storage and the initial upper layer storage function only before rainfall exceeding the maximum. Thus the two parameters model the phenomena of water detention and interception at the early stage.

Figure 3c illustrates the sensitivity of surface roughness (n). This parameter only controls the travel time of surface flow (i.e., surface flow velocity) but not the amount of
10   the three flows (not shown). Therefore the smaller n values induce more concentrated and faster flow to the outlet and vice visa.

For the remaining 5 parameters we plot the surface, inter and base flows separately to illustrate the effects as parameters change. Figure 3d.1~3, Fig. 3e.1~3, Fig. 3f.1~3, Fig. 3g.1~3, and Fig. 3h.1~3 represent the hydrograph responses in surface flow, inter
15   flow, and base flow as changing parameter m_i, D, K, m_b, and P, respectively. The parameter, m_i, mainly controls the shape of inter flow (Fig. 3d.2) with less effects on surface flow and base flow (Fig. 3d.1 and Fig. 3d.3). Higher m_i produces a faster response in inter flow and vice versa.

As D (Fig. 3e.1~3) changes, the responses of inter flow are significant. In general,
20   lower D means a smaller water storage in middle layer, and may cause a larger saturated area which enhances the surface flow (Fig. 3e.1), but diminishes the inter flow primarily (Fig. 3e.2). D affects base flow insignificantly. Parameter K also controls the inter flow in similar way as D does. However, surface flow is less affected by K whereas K's effect on base flow is more obvious (Fig. 3e.3). Parameter m_b has insignificant ef-
25   fects on surface and inter flows yet affects base flow significantly (Fig. 3g.1~3). The lower m_b produces a slower response of base flow, particularly, at the early stage.

Parameter P dominates the source of base flow. Lower P naturally decreases the base flow with simultaneous enhancement in the surface and inter flows. The lower P, in fact, represents the water may stay longer in middle layer, consequently, results

in higher inter and surface flows (Fig. 3h.2 and Fig. 3h.1). However, it should be kept in mind that the simulated hydrographs and quantities of the 3 components is derived from model and should be cross-validated by using chemical tracers or independent techniques in the future.

The influences of parameters on the total amounts of the 3 flows are examined by increasing and decreasing 10, 30, 50%, respectively, in each parameter. Figure 4 shows the responses of total discharge in surface flow, inter flow, and base flow, respectively, (in y-axis) against parameter changes (in x-axis). Obviously, D, K and m_i are the governing parameters showing strong positive correlation with total discharge. 1.0% of change in D, K, and m_i may give 0.27, 0.20, and 0.15% deviations in terms of total water discharge.

In surface flow component, D, P and K play negative feedbacks while m_i plays a positive one. For inter flow component, D and K are the most sensitive parameters and are positively correlated with the amount of inter flow. P is less sensitive comparing to D and K in controlling inter-flow, and it has negative effects. For base flow component, P has the largest and positive effect while K and D have smaller effects with negative correlations. Since the fractional contribution of interflow is as high as 48%, parameters dominate interflow responses reasonably act as the most sensitive ones though compensation effects appear among them.

4.2   Global best-fitted simulation and calibration

Simulations derived from the global best-fitted and the event best-fitted combination are compared by using the 5 indicators aforementioned (Table 3). For individual event, best-fitted EC varies from 84.5∼99.5% with an average EC of 93.6% while $EC_{\log}$ values range from 83.4 to 98.6% with an average of 90.6%. The means of absolute value of EQV and EQP are 5.3% and 5.6%, respectively. Generally speaking, we have quite high performances for each event which indicates near-perfect simulations can be achieved by specific combination. By contrast, EC values of simulations derived from global best-fitted set (n=0.037, $S_{1\,\max}$=20.0 mm, S_{10}=17.7 mm, m_i=49.2, D=1.07 m,

$K = 2.06$ m/h, $m_b = 116.48$, $P = 0.21$ mm/h) vary from 40.1 to 92.9% with an average of 75.1%, which is lower than independent simulations (Table 3). The global best-fitted set gives $EC_{\log}$ values from 69.0 to 96.6% with an average of 87.2%. Meanwhile, the means of absolute value of EQV and EQP are 12.2% and 18.3%, respectively. Though global best-fitted combination provides less satisfying result compared to that derived from event best-fitted combination, CRMSE takes all events into account and broadens the applicability of global best-fitted set for all events at a wide range of rainfall intensity.

Here we show all simulated hydrographs derived from the global best-fitted combination to reveal observed and simulated hydrograph features in Fig. 5. Four common features are revealed: First, for all events the observed discharge does not respond to rainfall at early stage. This phenomenon is typical in forestry watersheds due to water detention or interception caused by intensive vegetation. In our simulation, simulated hydrographs also do not respond to rainfall in the early stage. Second, the fact that both surface flow and interflow respond rapidly dominates the hydrograph. Surface flow dominates particularly under torrential and concentrated rainfall, such as event 2, 3, 7 and 14 (Fig. 5b, c, g and n), whereas, the inter flow dominates when the rainfall is relative small and gentle, such as Event 10 and 13 (Fig. 5j and m). Obviously, rainfall characteristics may manipulate the relative contribution of surface flow and interflow in model simulation. Third, the base flow, unlike the surface flow and interflow, always shows slow responses which occupy a small portion of total discharge. In addition, the largest (Event 2) and smallest (Event 13) events lay on the upper and lower ends of the range of calibration events (based on peak flow) just held the lowest 2 EQP values when the global best-fitted set was applied (discussed below).

4.3 Validation and inter-comparison among all events

For validation events by global best-fitted combination, simulation results are presented in Fig. 5o, p, q, r and the 5 indicators are listed in Table 4. The EC values vary from 63.2~90.5% with an average of 77.3%. The $EC_{\log}$ values range from 57.1~92.1% with an average of 79.1%. Meanwhile, the means of absolute values of EQV and EQP are

Printer-friendly Version

Interactive Discussion

12.2 and 19.8%, respectively, with ranges of $-22.5 \sim +13.1\%$ and $-39.5 \sim +9.9\%$.

The means of EC, $EC_{\log}$, EQV, and EQP for calibration events are 75.1, 87.2, -1.72, and -1.14, respectively, with standard deviations of 15.1, 7.0, 15.7, and 22.2 (Table 3). As mentioned earlier, calibration and validation events cover a sufficiently wide range of total rainfall and most validation events fall within ±1 standard deviation in term of respective indicator. In other words, the overall performances of validation events are similar to that of calibration events. Such agreement potentially allows us to apply our model in this subtropical watershed properly for future management.

We want to point out some of those simulations fall out of acceptable range of respective indicators. For example, Event 9 has lower EC value and higher EQV. In fact, Event 9, 2, 4, 10, 16 and 18 have multi peaks in precipitation pattern. However, for Event 9 and 18 their observed flood peaks are out of phase with the rainfall peak. Such decoupled rainfall-runoff response would not appear in our model. For the other multi peak events, flood peak always coincides with peak instantaneous precipitation (see Table 1). Real cause for this observed out-of-phase response remains unknown. Event 15 falls outside the standard deviation of $EC_{\log}$. The event is particularly short-lived with the highest maximum rainfall intensity, average rainfall intensity and peak flow (Table 1). Since it is short-lived, limited low discharge hours may bias the calculation indicator of $EC_{\log}$ mathematically. The simulations of Event 9 and Event 13 are obvious overestimations in EQV. Event 9 comes up with the reason mentioned above. The major overestimation of discharge is owing to the contribution of the first simulated discharge peak. Similarly, the observed discharge of Event 13 (Fig. 5m) does not respond significantly with the rainfall pattern in first rainfall peak that occurs at the 30th h; yet the simulated hydrograph presents a consistent result with the others. Event 16 (Fig. 5p) have a significant overestimation in EQV and EQP, respectively. The simulation of Event 16 (Typhoon Nari), which brings over 1000 mm rainfall causing extreme discharge of 15 241 cms, gives lower EC and EQP values of 74.5 and -39.5%, respectively.

Those unusual events somewhat can not be expected to comply with normal events;

whereas suffering the similar rainfall, the observed discharges may not be quite the same in the real world. For example, Reaney et al. (2007) used the ideal hillslope suffering different rainfall patterns with the same amount to investigate the hydrologic responses. They concluded that storms with similar amounts of total rainfall but with varying rainfall allocation can produce very different discharge amounts and peak flows depending on the storm characteristics. Pebesma et al. (2007) applied QPBRRM, a quasi-physically based rainfall-runoff model, on R-5 catchment with 72 rainfall-runoff events and concluded that event variables (e.g. total rainfall, rainfall intensity, runoff coefficient) can improve the model performance significantly. These two recent studies reveal that the influence of storm characteristics on runoff generation may not be interpreted completely in many modern models. Other reasons may be attributed to the uncertainty of rainfall measurements, model structure, and discharge measurements.

4.4 Peak water level prediction

To predict the peak flow caused by typhoon is crucial but always not easy (Sui et al., 2002; Li et al., 2005). Instead, water level rather than discharge is the important reference for embankment construction and flood mitigation. Here we transfer water discharge into water level to examine the predictive capability of our model in water level simulation, which is crucial in flood assessment. The simulated water discharge is converted into water level by using discharge-level relationship (rating curve) constructed by WRA in respective year. Except for Event 2 (-0.76 m) and Event 16 (-0.99 m) the deviation between predicted and observed peaks in water level are <0.4 m with most deviations <0.3 m. As for lager water level offsets in the Event 2 (Fig. 5b) and Event 16 (Fig. 5p), which are the largest two floods, we do not have sufficient information to prove their factuality. The rating curve method may be biased in high magnitude discharge owing to the fewer records. Besides, the channel cross section has been changed by extreme storms frequently, especially in Taiwan.

4.5 Confidence interval

The confidence intervals of simulated discharge are constructed on the basis of 14 calibration events. We classify the simulated discharges into 5 classes by interval of 100 cms (from 0 to 500 cms). In each category, probability distribution of relative ratio (Q_{obs}/Q_{sim}) is calculated. Here we like to emphasize all observed values should be compared with simulated values to present model predictive capability. The median, 95% upper limit and 5% lower confidence limit in each category is presented in Fig. 6. The medians of the 5 classes appear at 110, 87, 95, 99 and 125% of simulated discharge. The 90% confidence interval of the five classes are 52.0~216.7%, 33.3~166.1%, 43.7~119.1%, 66.9~147.3% and 96.2~154.6% of simulated discharge, respectively.

   Such confidence interval derived from multi events serves as a crucial reference for future hydrograph predictions. As Beven (2006) indicated that "we know that we have unknown errors in input and boundary conditions that get proceed non-linearly through a model that has structural errors and which is then compared with observations that have unknown measurement and commensurability error characteristics". Other than these ambiguous errors, manipulation of calibration also involves in model prediction (e.g. event weighting, performance measure selection). Despite of those unknown errors and their complex interactions that fog the simulation, all we urgently want to know in practical applications is the confidence of model simulations. Here we put validation events into the plot to examine properness of our confidence intervals. In Fig. 6, most of the observed discharges of validation events (red cross) are enveloped by the confidence intervals identified for the 5 water discharge classes. Note that the data points at high flow are obviously insufficient for confidence interval construction. With increasing data points, the medians and intervals can be constructed more robustly. Nevertheless, this comparison reveals the predictive capability of our model; meanwhile, the multi-event confidence interval identified by our procedure provides useful information for practical applications. The upper confidence limit is suggested prefer-

ably for flood risk assessment and the lower confidence limit preferably for drought assessment. With the improvements of measurements and understanding of model structure, the confidence intervals can be further refined and certainly improve the capacity of hydrological simulations.

5   Conclusions

This study demonstrates the capability of 3-layer TOPMODEL in simulating flood hydrograph induced by subtropical typhoon in a mountainous watershed in Taiwan. Sensitivity analysis reveals D (soil depth), K (hydraulic conductivity), and m_i (soil moisture decay) are major parameters to determine hydrograph shapes and total discharges. 1.0% of changes in D, K, and m_i may result in 0.27, 0.20, and 0.15% deviations in terms of total water discharge.

The global best-fitted combination gives an average performance of 75.1% in EC and 87.2% in $EC_{\log}$ for 14 calibration events and 77.3% in EC and 79.1% in $EC_{\log}$ for 4 validation events. When converting discharge to water level by rating curve, 16 of the eighteen events model predictions of peak water level are less than 40 cm, except two largest storms. Using comparison between observed and simulated discharges among all calibration events to construct confidence interval shows that most discharges of validation events fall inside the 90% confidence interval. The upper confidence limit is suggested preferably for flood assessment.

The study provides crucial information to modelers who are interested in TOPMODEL and other applications (e.g. flood forecasting, material flux estimating) in subtropical region. Meanwhile, it also extends three important issues: 1) the simulated surface flow, interflow, and base flow should be investigated by using chemical tracers in the future. Because the proportions of the three components in subtropical is rarely known; 2) the influence of storm characteristics on runoff generation should also be explored. Understanding the influence can cast lights on the improvement of model simulation. 3) The procedure of confidence interval estimation is valuable for develop-

Printer-friendly Version

Interactive Discussion

ing practical applications. The upper and lower confidence limits are direct aids to flood and drought assessments.

References

Beven, K. J.: TOPMODEL: a critique, Hydrol. Process., 11(9), 1069–1086, 1997.

Beven, K. J.: Parameter Estimation and Predictive Uncertainty, in: Rainfall-Runoff Modelling, edited by: Beven, K. J., The Primer, WILEY: New York, 217–253, 2001.

Beven, K. J.: On undermining the Science?, Hydrol. Process., 20, 3141–3146, 2006.

Campling, P., Gobin, A., Beven, K., and Feyen, J.: Rainfall-runoff modeling of a humid tropical catchment: the TOPMODEL approach, Hydrol. Process., 16(2), 231–253, 2002.

Candela, A., Noto, L. V., and Aronica, G.: Influence of surface roughness in hydrological response of semiarid catchments, J. Hydrol., 313, 119–131, 2005.

Casadei, M., Dietrich, W. E., and Miller, N. L.: Testing a model for predicting the timing and location of shallow landslide initiation in soil mantled landscapes, Earth Surf. Proc. Land., 28(9), 925–950, 2003.

De Smedt, F., Liu, Y. B., and Gebremeskel, S.: Hydrological modeling on a catchment scale using GIS and remote sensed land use information, in: Risk Analysis II, edited by: Brebbia, C. A., WTI press, Southampton, Boston, 295–304, 2000.

Günter, A., Uhlenbrook, S., Seibert, J., and Leibundgut, C.: Multi-criterial validation of TOPMODEL in a mountainous catchment, Hydrol. Process., 13 1603–1620, 1999.

Hamon, W. R.: Estimating potential evatranspiration. Proceedings of the American Society of Civil Engineering, ASCE Proceedings J. Hydraulics Division, 87(HY3), 107–120, 1961.

Hornberger, G. M., Scanlon, T. M., and Raffensperger, J. P.: Modelling transport of dissolved silica in a forested headwater catchment: the effect of hydrological and chemical time scales on hysteresis in the concentration-discharge relationship, Hydrol. Process., 15(10), 2029–2038, 2001.

Huang, J. C., Kao, S. J., Hsu, M. L., and Lin, J. C.: Stochastic procedure to extract optimal input

An integrated 3-layer TOPMODEL

Jr-Chuan Huang et al.

parameter combinations and to construct integrated landslide occurrence map: An example of mountainous watershed in Taiwan, Nat. Hazards Earth Syst. Sci. 6 803–815, 2006.

Krause, P., Boyle, D. P., and Bäse, F.: Comparison of different efficiency criteria for hydrological model assessment, Adv. Geosci., 5 89–97, 2005.

5 Lamb, R. and Beven, K. J.: Using interactive recession curve analysis to specify a general catchment storage model, Hydrol. Earth Syst. Sci., 1, 101–113, 1997.

Lamb, R., Beven, K., and MyrabØ, S.: A generalized topographic-soils hydrological index, in: Landform Monitoring, Modeling and Analysis, edited by: Lans, S. N., Richards, K. S., and Chandler, J. H., John Wiley: Chichester, 263–278, 1998.

10 Li, M. H., Yang, M. J., Soong, R., and Huang, H. L.: Simulating typhoon floods with gauge data and mesoscale modeled rainfall in a mountainous watershed, J. Hydrometeorol., 6(3), 306–323, 2005.

Liu, Y. B., Gebremeskel, S., De Smedt, F., Hoffman, L., and Pfister, L.: A diffusive approach for flow routing in GIS based flood modeling, J. Hydrol., 283, 91–106, 2003.

15 Madsen, H.: Automatic calibration of a conceptual rainfall-runoff model using multiple objectives, J. Hydrol., 235, 276–288, 2000.

Molnar, P. and Ramirez, J. A.: Energy dissipation theories and optimal channel characteristics of river network, Water Resour. Res., 34(7) 1809–1818, 1998.

Monteith, J. L.: Evaporation and environment, Symposia of the Society for Experiment Biology,
20 19, 205–234, 1965.

Nash, J. E. and Sutcliffe, J. V.: River flow forecasting through conceptual models 1. A discussion of principles, J. Hydrol., 10 282–290, 1970.

Pebesma, E. J., Switzer, P., and Loague, K.: Error analysis for the evaluation of model performance: rainfall-runoff event summary variables, Hydrol. Process., 21(22), 3009–3024,
25 2007.

Penman, H. L.: Natural evaporation from open water, bare soil, and grass, P. R. Soc. London, 193, 120–195, 1948.

Reaney, S. M., Bracken, L. J., and Kirkby, M. J.: Use of the connectivity of runoff model (CRUM) to investigate the influence of storm characteristics on runoff generation and connectivity in
30 semi-arid areas, Hydrol. Process., 21, 894–906, 2007.

Scanlon, T. M., Raffensperger, J. P., and Hornberger, G. M.: Shallow subsurface storm flow in a forested headwater catchment: Observations and modeling using a modified TOPMODEL, Water Resour. Res., 36(9), 2575–2586, 2000.

An integrated 3-layer TOPMODEL

Jr-Chuan Huang et al.

Singh, V. P.: Effect of spatial and temporal variability in rainfall and watershed characteristics on stream flow hydrograph, Hydrol. Process., 11, 1649–1669, 1997.

Sui, C. H., Huang, C. Y., Tsai, Y. B., Chen, C. S., Lin, P. L., Shieh, S. L., Li, M. H., Liou, Y. A., Wang, T. C. C., Wu, R. S., Liu, G. R., and Chu, Y. H.: Meteorology-hydrology study targets Typhoon Nari and Taipei Flood, EOS, Trans. Amer. Geophys. Union, 83(24), 265–270, 2002.

Tarboton, D. G.: A new method for the determination of flow directions and con tributing areas in grid digital elevation models, Water Resour. Res., 33(2), 309–319, 1997.

Walter, M. T., Steenhuis, T. S., Mehta, V. K., Thongs, D., Zion, M., and Schneiderman, E.: Refined conceptualization of TOPMODEL for shallow subsurface flows, Hydrol. Process., 16, 2041–2046, 2002.

Wang, Y. C., Han, D., Yu, P. S., and Cluckie, I. D.: Comparative modeling of two catchments in Taiwan and England, Hydrol. Process., 20(20), 4335–4349, 2006.

Wu, L., Wang, B., Geng, S.: Growing typhoon influence on east Asia, Geophys. Res. Lett., 32, L18703, doi:10.1029/2005GL022937, 2005.

Zevenbergen, L. W. and Throne, C. R.: Quantitative analysis of land surface topography, Earth Surf, Proc, Land,, 12, 47–56, 1987.

An integrated 3-layer TOPMODEL

Jr-Chuan Huang et al.

Title Page

Abstract	Introduction
Conclusions	References
Tables	Figures

◄ | ►

◄ | ►

Back | Close

Full Screen / Esc

Printer-friendly Version

Interactive Discussion

Table 1. The basic characteristics of the 18 events during 1990–2004 in Heng-Chi watershed.

Event number	Date	Rainfall (mm)	Rainfall time (h)	Avg. RI (mm/h)	Max. RI (mm/h)	Total discharge (cms)	Peak flow (cms)	Lag time (h)
No. 1	1990/09/18	342	40	8.6	48.0	4720.3	492.0	1
No. 2	1990/08/30	316	24	13.2	51.0	4702.4	668.0	1
No. 3	1990/09/07	252	39	6.5	20.0	3562.1	290.0	0
No. 4	1991/08/17	210	23	9.1	46.0	2118.2	126.0	19
No. 5	1992/08/27	500	77	6.5	20.0	5344.3	149.0	1
No. 6	1993/06/05	146	15	9.7	54.0	1648.1	179.0	1
No. 7	1996/07/30	450	42	10.7	31.0	3475.8	243.0	1
No. 8	1997/08/17	223	32	7.0	22.0	2223.9	195.0	7
No. 9	1997/08/28	195	25	7.8	24.0	1386.0	132.0	8
No. 10	1998/10/04	306	52	5.9	36.0	2718.4	117.0	14
No. 11	1998/10/15	475	36	13.2	36.0	4062.2	174.0	0
No. 12	2000/08/26	81	8	10.1	35.0	723.18	77.0	0
No. 13	2000/08/28	204	36	5.7	25.0	1575.9	68.6	1
No. 14	2000/10/31	508	46	11.0	33.0	6054.3	317.0	1
*No. 15	2001/06/16	125	6	20.8	61.0	869.1	310.0	1
*No. 16	2001/09/16	1026	62	16.5	58.0	15241.1	870.0	2
*No. 17	2004/07/04	114	10	11.4	30.0	1381.3	232.3	2
*No. 18	2004/09/11	486	46	10.6	33.0	5113.4	245.9	0
Avg.	–	331.1	34.4	10.2	36.8	3717.8	271.4	–

*   means event for validation;
Avg. RI   means the average rainfall intensity;
Max. RI   means the maximum rainfall intensity.

Table 2. The description, sampling range, and distribution of the 8 input parameters.

parameter	definition and unit	range	Distribution
n	Surface roughness, (–)	0.025~0.05	Uniform
$S_{1\,max}$	The maximum available upper layer storage, (mm)	1.0~50.0	Uniform
S_{10}	The initial upper layer storage, (mm)	1.0~50.0	Uniform
m_i	Soil characteristic parameter indicating soil moisture decay, (–)	40~100	Uniform
D	Soil depth, (m)	0.5~3.0	Uniform
$Log(K)$	Hydraulic conductivity, (m/h)	−3.0~1.0	Uniform
m_b	The recession coefficient of base flow, (–)	80~200	Uniform
P	The percolation rate, (mm/d)	0.2~6.0	Uniform

An integrated 3-layer TOPMODEL

Jr-Chuan Huang et al.

Table 3. the five indicators of the simulations among the 14 events using the individual and global best-fitted set.

Event number	EC (%)		EC_{log} (%)		EQV (%)		EQP (%)		EPT (h)
	Individual	Global	Individual	Global	Individual	Global	Individual	Global	Global
No. 1	93.3	87.5	91.2	89.5	−8.2	−14.1	−9.7	−18.3	1
No. 2	90.6	82.9	83.4	83.2	−17.6	−18.5	−22.9	−35.1	0
No. 3	91.0	76.0	89.4	69.0	−11.1	−12.8	−9.5	−28.4	1
No. 4	91.8	61.5	94.4	83.3	−3.2	−21.9	−2.5	−13.3	1
No. 5	84.5	60.8	91.6	80.2	−1.8	+6.3	−1.9	+12.8	0
No. 6	97.8	84.5	91.3	88.8	+0.8	−20.3	0.0	+8.0	0
No. 7	96.9	91.7	86.9	92.2	+5.0	0.0	−7.0	−12.0	0
No. 8	97.8	65.4	86.9	86.9	−7.6	+6.9	−4.4	+11.8	−2
No. 9	93.6	40.1	84.6	92.7	+3.5	+32.3	0.0	+23.3	0
No. 10	93.3	88.3	94.5	93.6	+1.2	+2.2	−7.5	−4.0	0
No. 11	91.3	81.7	95.6	88.6	−5.8	−7.9	+9.8	+16.7	0
No. 12	98.3	73.7	93.5	91.5	+4.6	−2.1	+0.8	−25.0	1
No. 13	91.1	63.7	86.8	84.0	+2.7	+20.7	+0.4	+43.6	1
No. 14	99.5	92.9	98.6	96.6	−1.1	+5.1	+1.9	+4.0	−1
Avg.	93.6	75.1	90.6	87.2	|5.3|*	|12.2|*	|5.6|*	|18.3|*	–

* means the absolute difference.

Table 4. The simulations of validated events by the global best-fitted set.

Event number	EC (%)	EC_{log} (%)	EQV (%)	EQP (%)	EPT (h)
No. 15	63.2	57.1	+9.95	−5.9	0
No. 16	74.5	85.4	−22.5	−39.5	0
No. 17	90.5	92.1	−3.3	−23.7	0
No. 18	81.1	81.9	+13.1	+9.9	0
Avg.	77.3	79.1	|12.2|*	|19.8|*	−

* means the absolute difference.

An integrated 3-layer TOPMODEL

Jr-Chuan Huang et al.

Table 5. The observed and simulated peak flows, water levels and differences.

Event number	Obs. peak flow (cms)	Obs. water level (m)	Sim. peak flow (cms)	Sim. water level (m)	Difference (m)
No. 1	492.0	25.04	402.0	24.72	−0.32
No. 2	668.0	25.59	433.5	24.83	−0.76
No. 3	290.0	24.26	207.6	23.88	−0.39
No. 4	126.0	23.42	109.2	23.31	−0.11
No. 5	149.0	23.56	168.1	23.67	0.11
No. 6	179.0	23.73	193.3	23.80	0.08
No. 7	243.0	24.05	213.8	23.91	−0.14
No. 8	195.0	23.81	218.0	23.93	0.12
No. 9	132.0	23.45	162.8	23.64	0.18
No. 10	117.0	23.36	112.3	23.33	−0.03
No. 11	174.0	23.70	203.1	23.85	0.15
No. 12	77.0	23.07	57.8	22.92	−0.16
No. 13	68.6	23.01	98.5	23.23	0.23
No. 14	317.0	24.38	329.7	24.43	0.05
No. 15	310.0	24.35	291.8	24.27	−0.08
No. 16	870.0	26.14	526.4	25.15	−0.99
No. 17	232.3	24.00	177.2	23.72	−0.28
No. 18	245.9	24.07	270.2	24.18	0.11
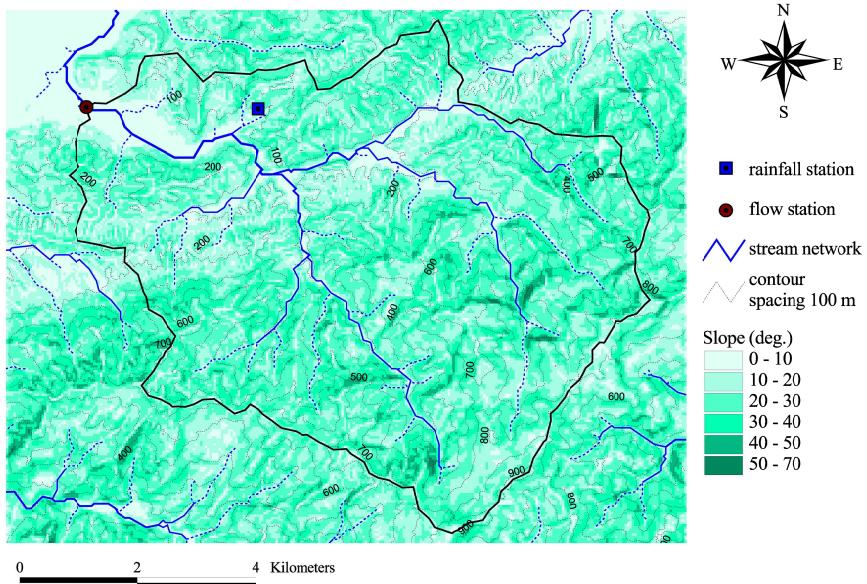
Fig. 1. The Heng-Chi watershed, stream network, elevation contour, slope, and hydrological stations.
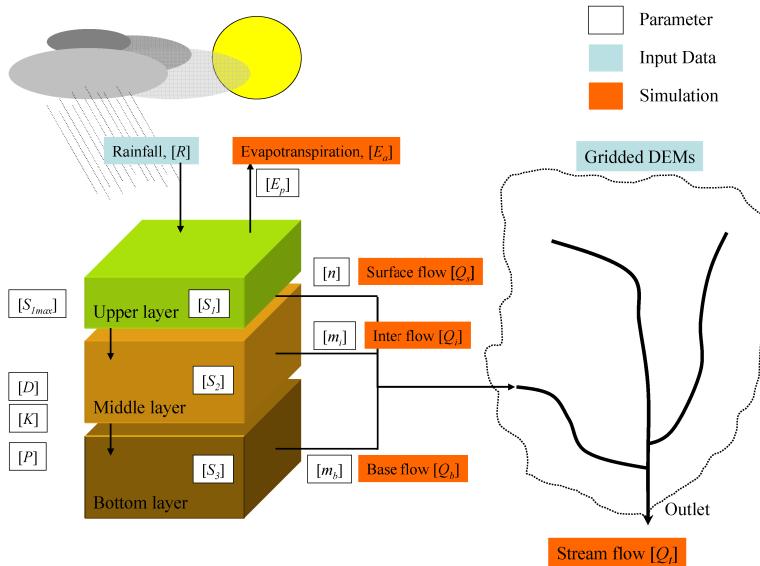
Fig. 2. Schematic diagram of the 3-layer TOPMODEL.

Full Screen / Esc
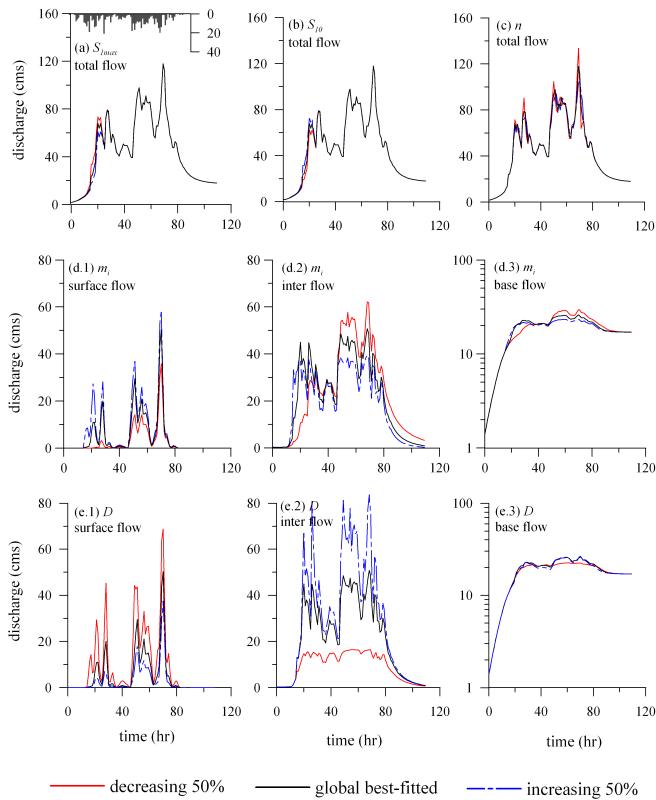
Fig. 3. The results of sensitivity analysis by using Event 5 by changing ±50% of each parameter based on the global best-fitted combination. The solid line shows the simulated hydrographs; dash red line and blue line, respectively, represent the results of decreasing and increasing 50% of each parameter value. Panels **(a)**, **(b)**, and **(c)** represent the total hydrographs as changing $S_{1\,max}$, S_{10}, and n, respectively. Panels (d.1~3) and panels (e.1~3) show the simulations of surface flow, inter flow, and base flow when changing parameter m_i and D, respectively.
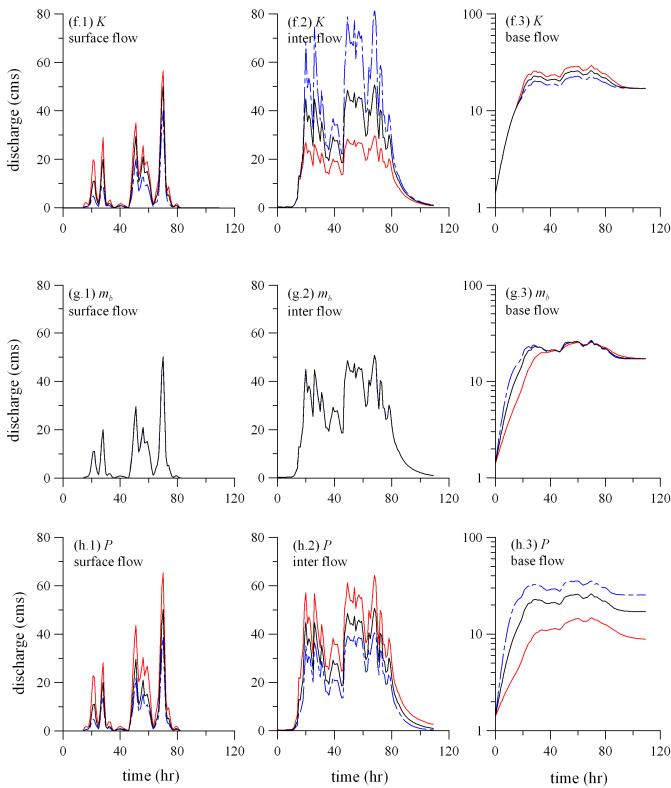
Fig. 3. Continued.
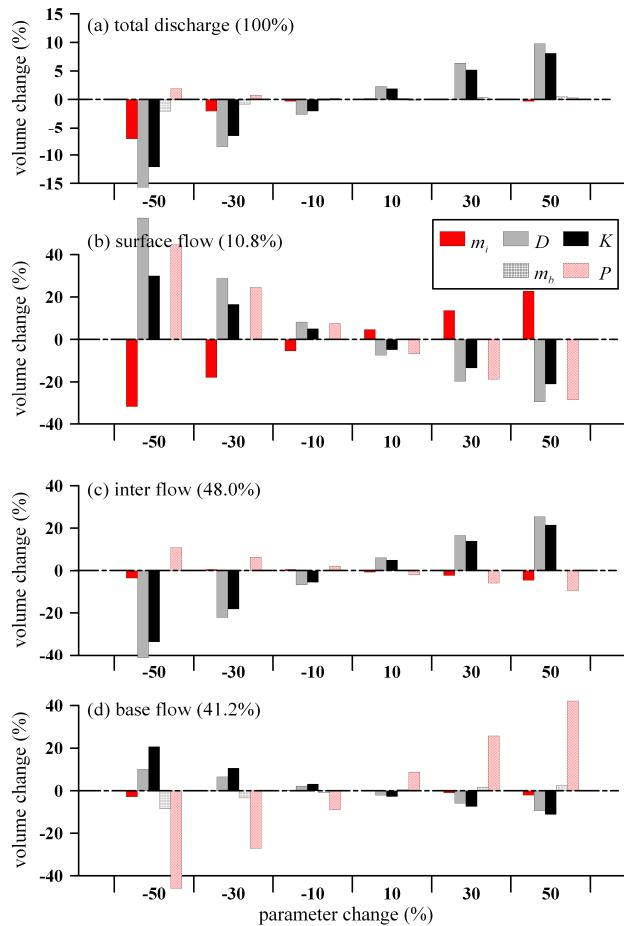
Fig. 4. The histograms of volume change (%) versus parameter change (%). The x-axis presents the percentage of parameter change over the global best-fitted combination and the y-axis shows the volume change comparing to the global best-fitted simulation.

HESSD

5, 1101–1135, 2008

An integrated 3-layer TOPMODEL

Jr-Chuan Huang et al.

Title Page

Abstract | Introduction

Conclusions | References

Tables | Figures

◀ | ▶

◀ | ▶

Back | Close

Full Screen / Esc

Printer-friendly Version

Interactive Discussion
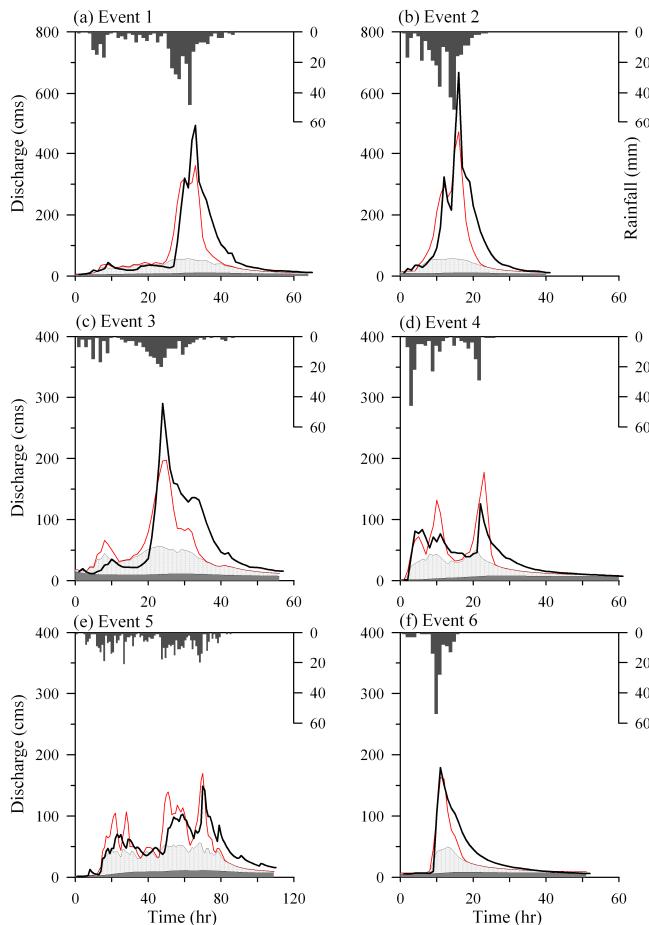
Fig. 5. The simulated and observed hydrographs with corresponded hyetographs of the 18 rain storms. The black solid line means the observed discharge; the red line represents the simulated total discharge; the gray-dot and shaded areas mean the simulated inter flow and simulated base flow, respectively.
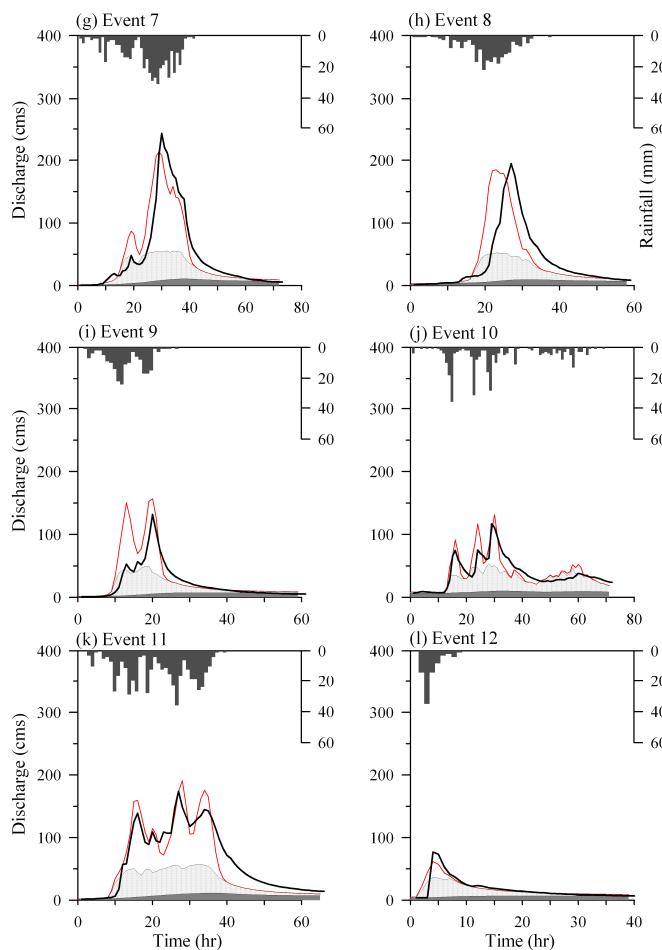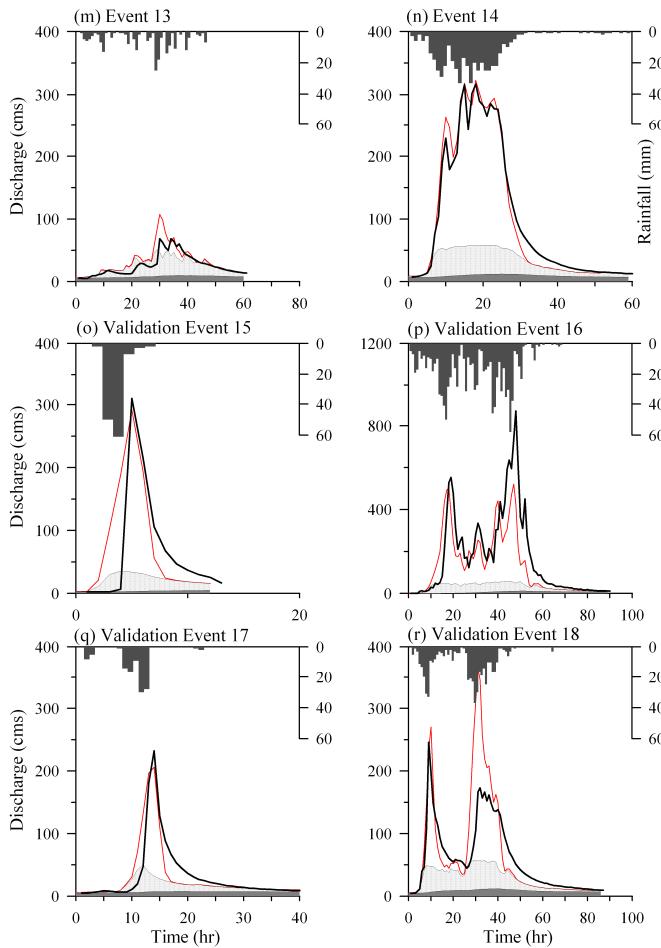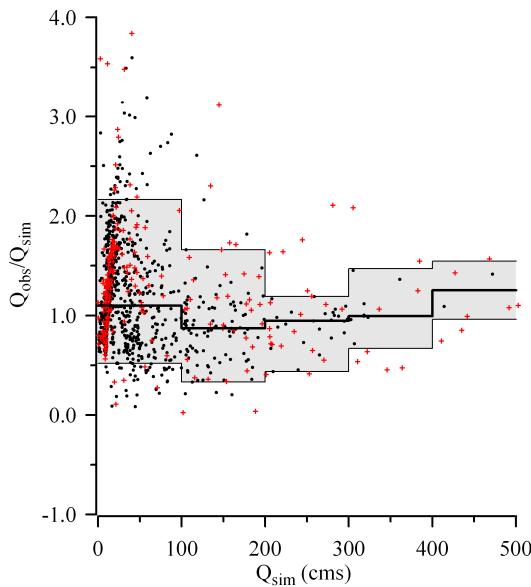
Fig. 5. Continued.

Fig. 5. Continued.

Fig. 6. the scatter plots of the Q_{obs}/Q_{sim} against Q_{sim}. The black circle and red cross markers represent the calibration and validation events. The black lines and the gray zones are the median and 90% confidence interval derived from all calibration events.